Radionuclide Emission Computed Tomography of the Head with ^{99m}Tc and a Scintillation Camera

Ronald J. Jaszczak, Paul H. Murphy, Diane Huard, and John A. Burdine

Searle Analytic Inc. and Searle Radiographics Inc., Des Plaines, Illinois, and St. Luke's Episcopal–Texas Children's Hospitals, Baylor College of Medicine, Houston, Texas

To investigate the potential application of radionuclide computed tomography (RCT) to nuclear medicine imaging using ^{99m}Tc, a tomographic system using a lightweight scintillation camera for brain imaging was constructed, and lesion contrast with RCT and conventional scintigraphy were compared. The detector revolves once around the patient's head at constant angular velocity, requiring approximately 20 min. Nine sections are reconstructed from the data, using either a Fourier transform or a filtered backprojection algorithm. In a phantom simulating the radionuclide distribution observed during brain imaging, quantitative lesion contrast was far superior in the RCT images. In a series of 25 patients with intracranial lesions, the average RCT lesion contrast was superior to that of standard scintigraphy by a factor of more than 2. An RCT image of an experimentally infarcted dog's heart, taken after the injection of ^{99m}Tc-MAA into the left atrium, also showed excellent correspondence to the gross anatomic defect. Although problems of photon absorption may occur in imaging larger body areas, RCT imaging in this feasibility study produced surprisingly good results that warrant further investigation of the technique.

J Nucl Med 18: 373–380, 1977

During the past few years, x-ray computed tomography has had a major impact on diagnostic imaging as a result of the work of Hounsfield and Ambrose (*1,2*). In 1963, Kuhl used gamma radiations in a similar tomographic technique that did not require a computer for image reconstruction (*3*). During the subsequent evolution of radionuclide computed tomography (RCT), the problems encountered included those relating to the specialized nature of the instrumentation, cumbersome mathematical manipulations, the necessity for rotating the patient on a constant axis, inadequate spatial resolution, wide random fluctuation in the data, and deficiencies in the reconstruction algorithms. These problems have been largely overcome in recent years, and the potential application of RCT to clinical nuclear medicine has been shown with considerable success. The results obtained with positron tomography, for example, have successfully validated the use of substrates labeled with radioactive carbon and nitrogen for monitoring certain aspects of human physiology and metabolism. Summaries of relevant publications on reconstruction tomography have been presented by Budinger (*4*) and by Brooks and DiChiro (*5*), and current approaches to RCT design have been recently described by Kuhl et al. (*6*), Muehllehner et al. (*7*), and Hoffman et al. (*8*).

The scintillation camera has also been used with ^{99m}Tc to obtain RCT sections by Keyes et al. (*9*)

Received July 19, 1976; revision accepted Nov. 19, 1976.

For reprints contact: John A. Burdine, Nuclear Medicine Sect., Dept. of Radiology, Baylor College of Medicine, Houston, TX 77030.

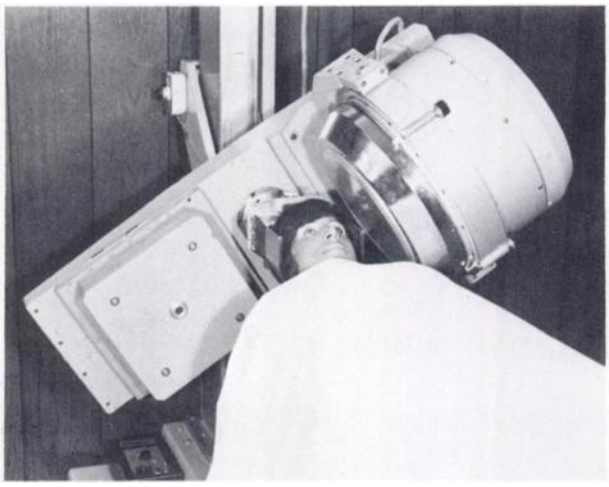

FIG. 1. RCT detector arrangement.

and others (*4,10–13*). Data are collected at appropriate angular increments about the patient and used for subsequent reconstruction of images of several parallel sections. In comparison with positron tomography, the practical advantage of this technique is its compatibility with widely available radiopharmaceuticals used in scintillation camera imaging. By contrast, photon-attenuation correction with RCT is more difficult than with positron tomography. To investigate further the potential clinical usefulness of RCT with low-energy gamma-emitters, a tomographic system using a lightweight scintillation camera was constructed to compare lesion contrasts obtained with RCT and with conventional scintigraphy.

INSTRUMENTATION AND METHODS

The camera assembly and head support are shown in Fig. 1. To simplify the mechanical engineering, this device was designed for brain imaging only. In this preliminary study, RCT views were obtained at the time of routine brain imaging with no additional radioactivity administered. The detector makes a single 360° revolution about the patient's head; it travels at constant angular velocity with continuous data collection. Using a standard medium-resolution low-energy collimator, this requires 20 min. This data-collection time was judged to be optimal after review of a series of images differing in total counts. Scintillation events are recorded on videotape along with a detector-orientation signal every 4° for subsequent off-line image reconstruction using a small

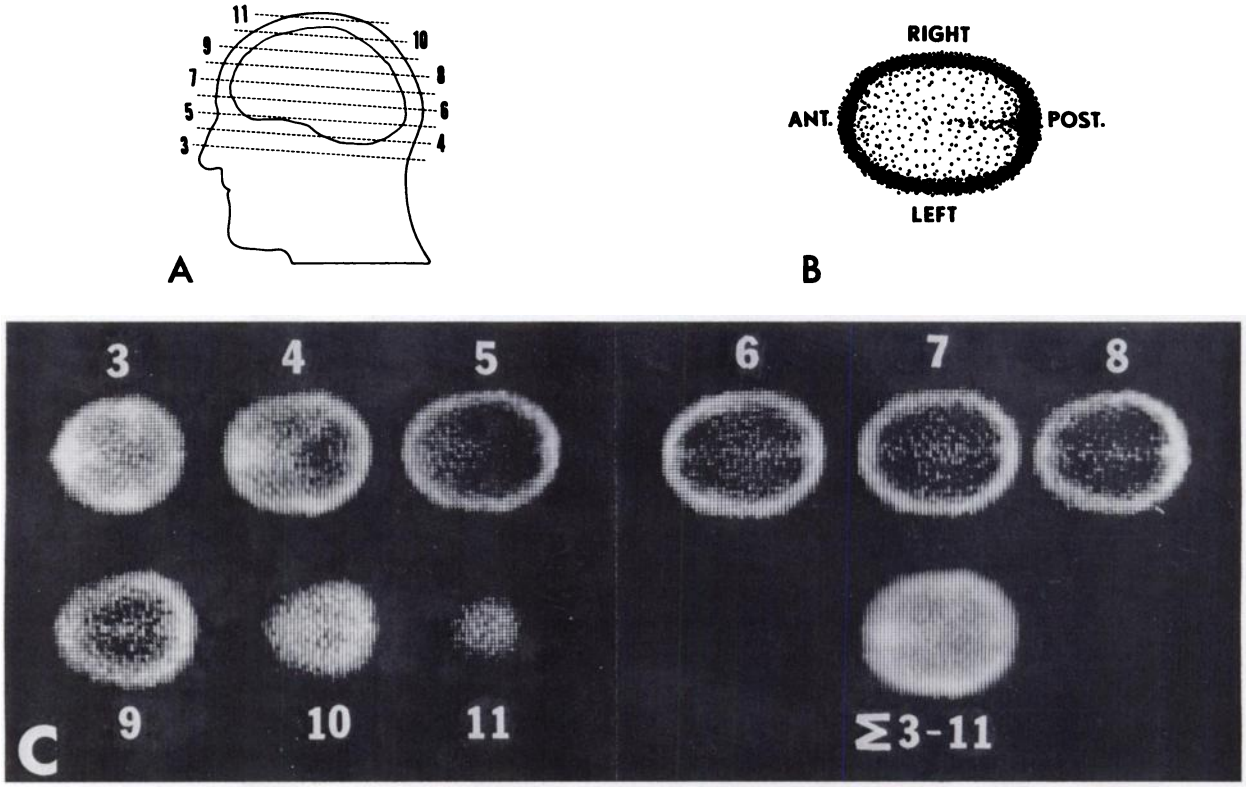

FIG. 2. (A) Midplanes of all nine tomographic sections. (B) Orientation of each section as displayed in reconstructed image. (C) Results from normal patient, obtained after 20 min of data collection at 1 hr after injection of 15 mCi of pertechnetate. Last image is summation of all nine levels.

computer. Typically, nine cross sections of the brain are reconstructed from the data: approximately 4,000,000 total counts, or 250,000 counts per section in the midbrain region are obtained with an average dose of 15 mCi of ^{99m}Tc. The midplanes of these nine sections are diagrammed in Fig. 2A for anatomic orientation. Each image represents a section thickness of 16 mm and the lateral resolution with ^{99m}Tc is about 14 mm (FWHM), compared with the 9 mm intrinsic resolution of the camera head in the nontomographic mode. The RCT sections are displayed and a summation image of all nine levels is also computed (Figs. 2B and 2C).

RECONSTRUCTION TECHNIQUES

Analytic rather than iterative methods were used for image reconstruction. Both Fourier transform and filtered back-projection algorithms were investigated, but the clinical images did not suggest any clear preference. The Fourier transform method used in this work is described by Kay et al. (*11*) and others (*14,15*). Several methods of interpolating the sampled polar data onto a Cartesian coordinate system in frequency space are possible. We used the four-point linear interpolation method described by Mersereau and Oppenheim (*16*). An interesting effect of this interpolation method in frequency space is the resulting roll-off in the spatial domain that occurs toward the edge of the field of view. The filtered back-projection method was based on the computer program presented by Brooks and DiChiro (*5*) and incorporates an interpolation scheme to obtain back-projection values lying between the sampled data points. Processing is accomplished in the spatial domain, using a convolution integral derived by Bracewell and Riddle (*17*). Since reconstructed images are not quantitative due to photon attenuation and scattering and differences in spatial resolution along a given ray, the geometric mean of opposing views was used to compensate partially for these effects.

Regardless of which method of reconstruction is used, certain fundamental parameters influencing resolution must be considered in constructing and implementing an RCT system. The matrix size is determined by the maximum spatial frequency that can be processed by the camera. A 64 × 64 digital matrix covering the 23-cm-diam field of view is adequate to preserve the spatial resolution of this system. The theoretically optimum angular-sampling increment for an object equal in diameter to the detector field of view is 2.5° (*18*), but no degradation in RCT image quality was observed for sampling increments up to 4°.

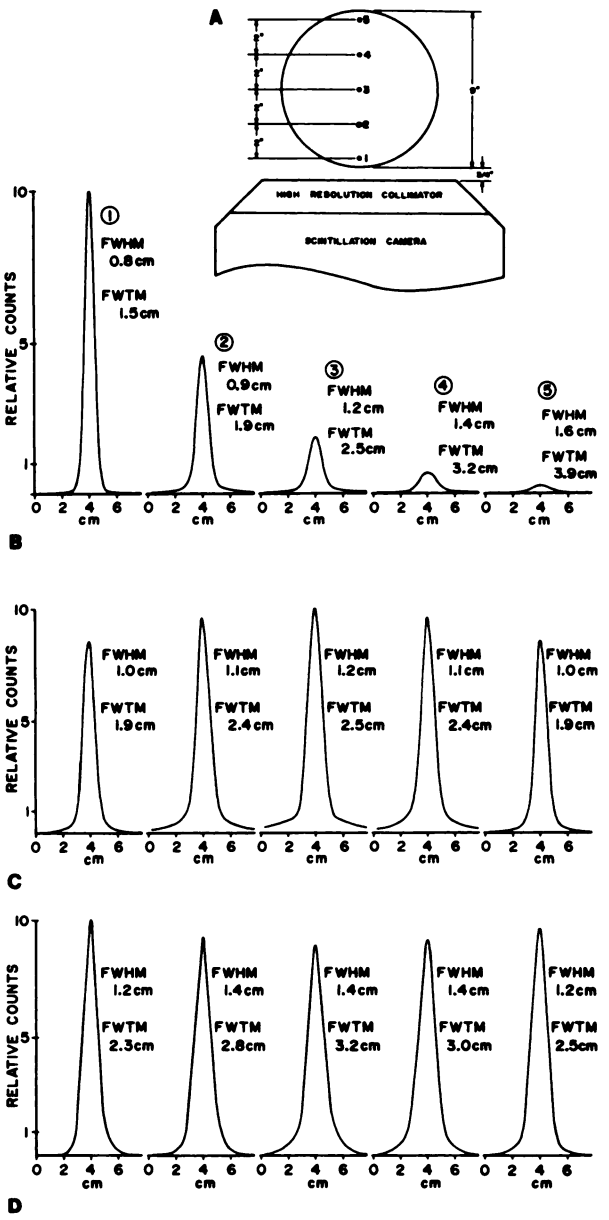

FIG. 3. Line sources containing ^{99m}Tc were imaged at five different locations within water-filled 9-in.-diam phantom to compare spatial resolution and sensitivity. Locations of five sources are shown in (A). (B) Line spread functions, normalized to peak counting rate at position 1, are shown for single-projection data collection. Line spread functions were obtained independently using one line source moved to each location. Notice rapid degradation of spatial resolution, reflected in increasing full width at half maximum (FWHM) and full width at tenth maximum (FWTM) and in rapid decrease in sensitivity with depth. (C) Use of geometric mean obtained from opposing views of line source may improve uniformity of resolution and sensitivity, as illustrated here. (D) By use of Fourier transform method, RCT reconstructions of line sources imaged at all five locations simultaneously illustrate good uniformity of resolution and sensitivity. Contributing influence was interpolation method used, which results in roll-off in values toward edge of field of view.

From an engineering standpoint, continuous rather than discrete detector motion is simpler and more reliable. Although the detector head of the RCT

system moves continuously about the patient, data are summed into 4° frames. This results in a smearing of projection data within each angular interval. In a direct comparison with discrete 4° sampling, however, there was no significant difference in image quality.

The random variations in the data in each reconstructed image are related to the total sampling time and the radioactivity in the patient. An angular velocity of 18°/min, corresponding to a data-collection time of 20 min, was routinely employed in patient imaging to permit collection of about 4,000,000 total counts from the entire field of view of the detector. This yields approximately 250,000 counts per reconstructed image.

IMAGING RESULTS

Line spread functions were measured as a function of depth with the camera in the RCT mode, and in the nontomographic mode for a single view and for opposing views using the geometric mean (Fig. 3). In the RCT mode only small changes in spatial resolution and sensitivity are evident across the field of view.

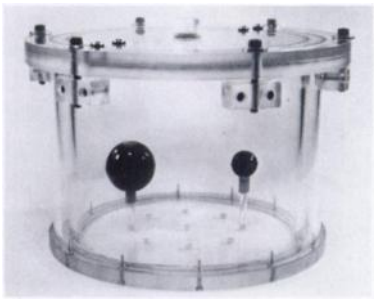

FIG. 4. Cylindrical phantom containing two spheres. Sleeve of increased activity was added at periphery to simulate brain imaging.

To obtain a quantitative comparison of lesion contrast, a cylindrical phantom containing two spheres was imaged in the stationary and RCT modes with the same camera system (Fig. 4). A sleeve of increased activity was added to the periphery of the phantom to simulate the radionuclide distribution present during brain imaging. Line profiles through the internal spheres provide an indication of lesion-to-background ratios. In Fig. 5A, the simulated le-

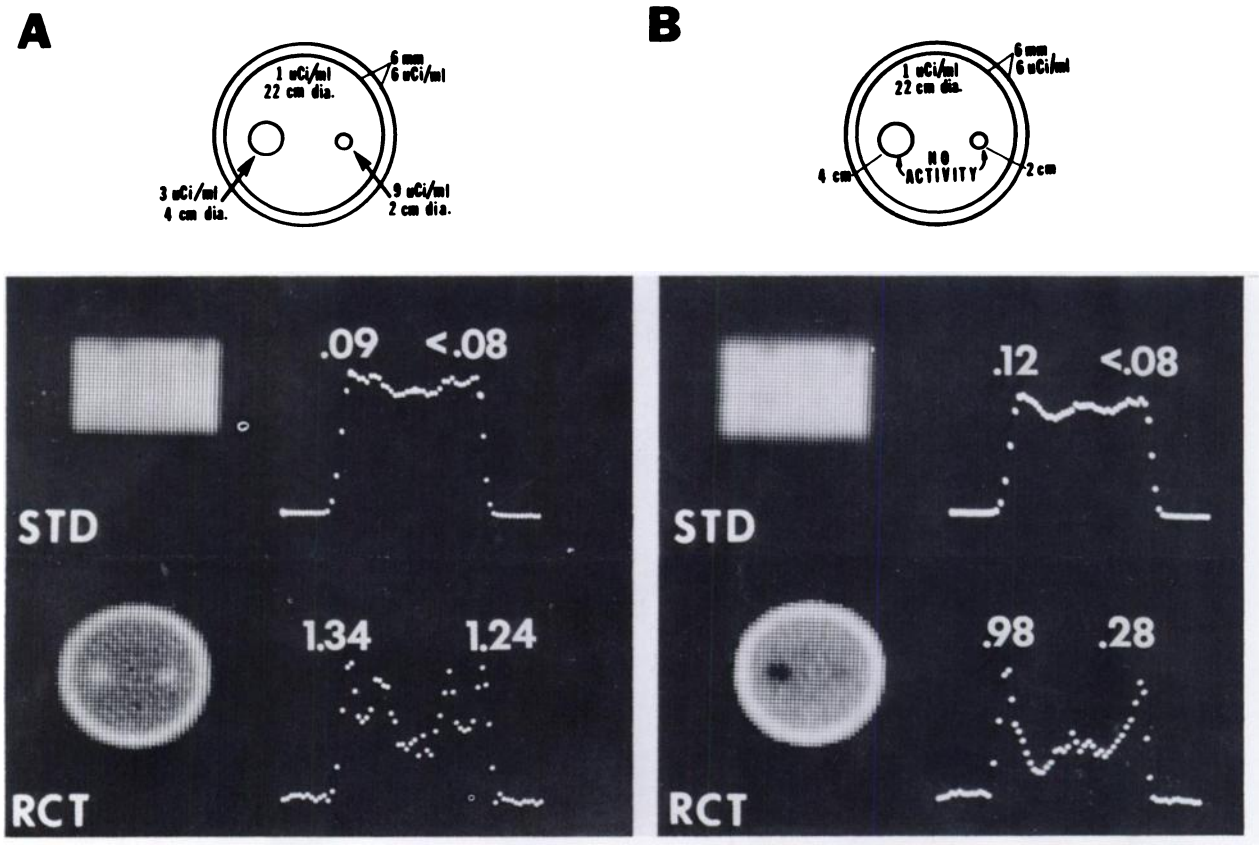

FIG. 5. Phantom-imaging results, with spheres containing increased activity (A) and no activity (B). Standard scintigrams and adjacent line profiles fail to provide significant lesion contrast in comparison with RCT images and profiles. Lesion-to-background ratios are shown above each line profile for both standard scintigrams and RCT images.

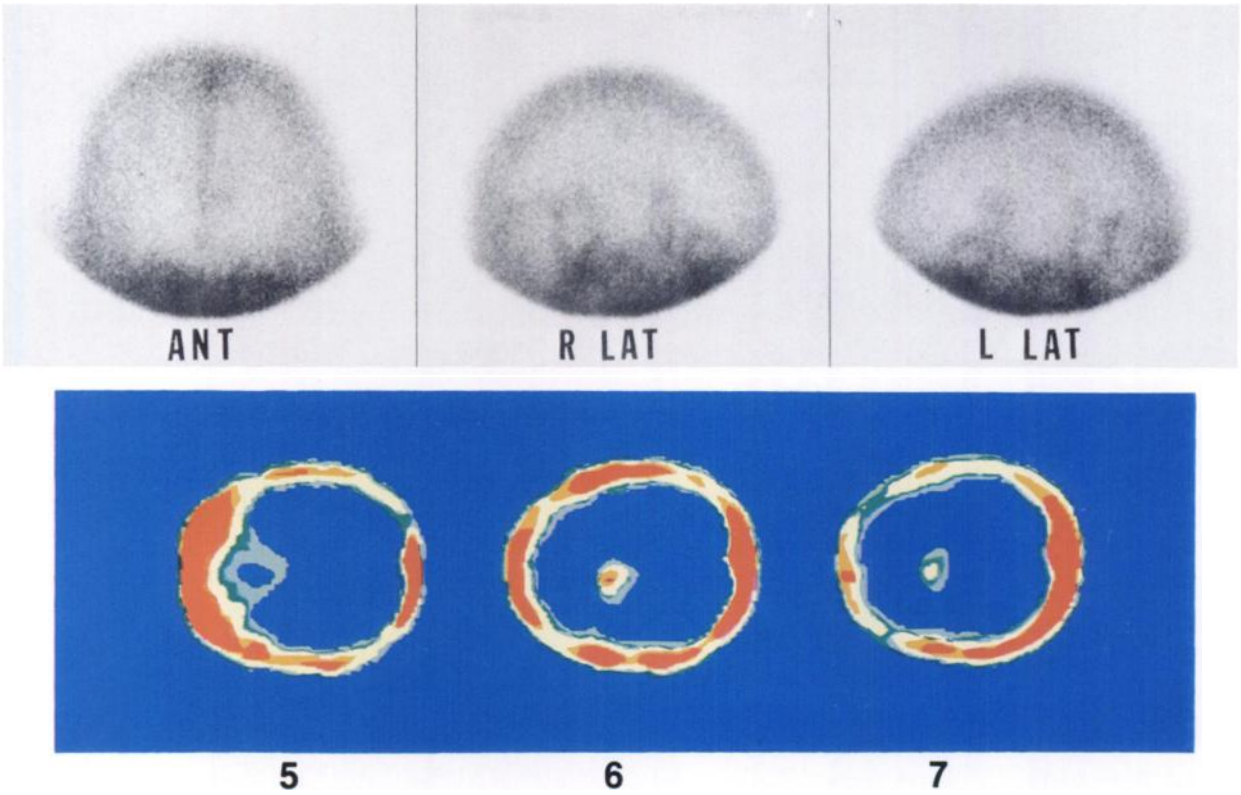

FIG. 6. 46-year-old man. Carcinoma metastatic from lung.

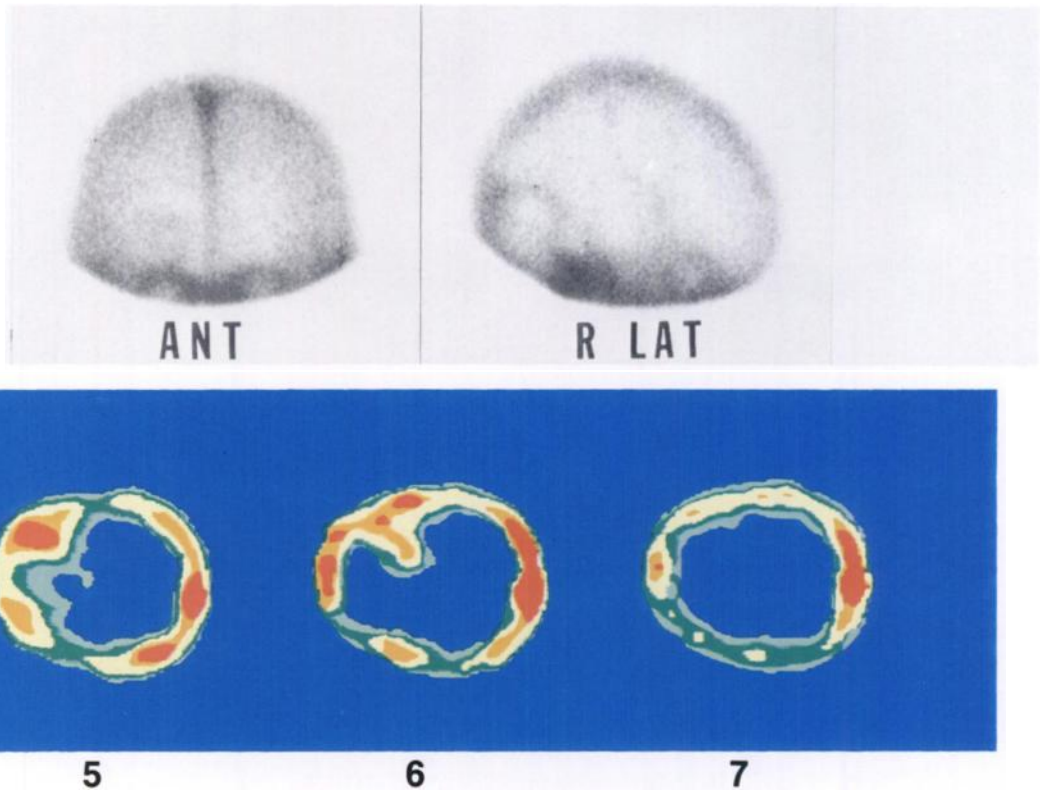

FIG. 7. 12-year-old girl. Knife wound, right orbit. Brain penetration was not suspected.

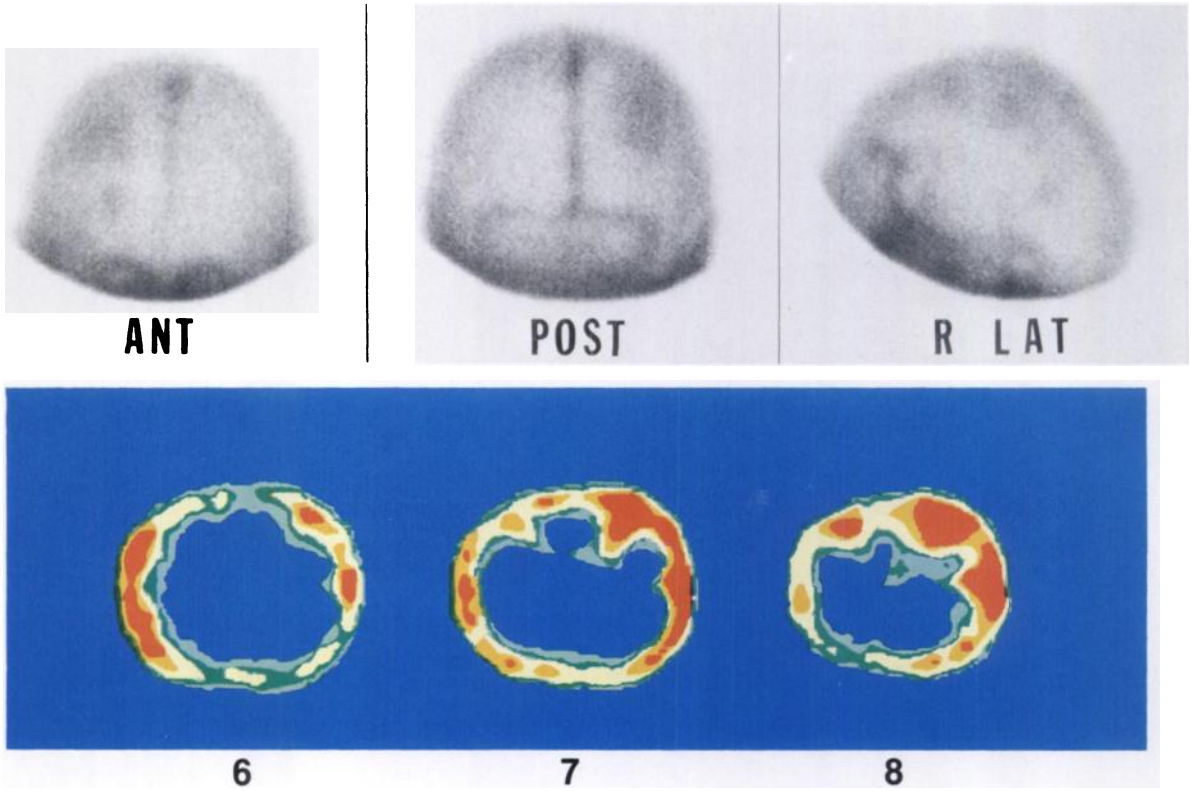

FIG. 8. Seventy-five-year-old woman. Right CVA. Contiguous nature of lesion is shown on RCT images.

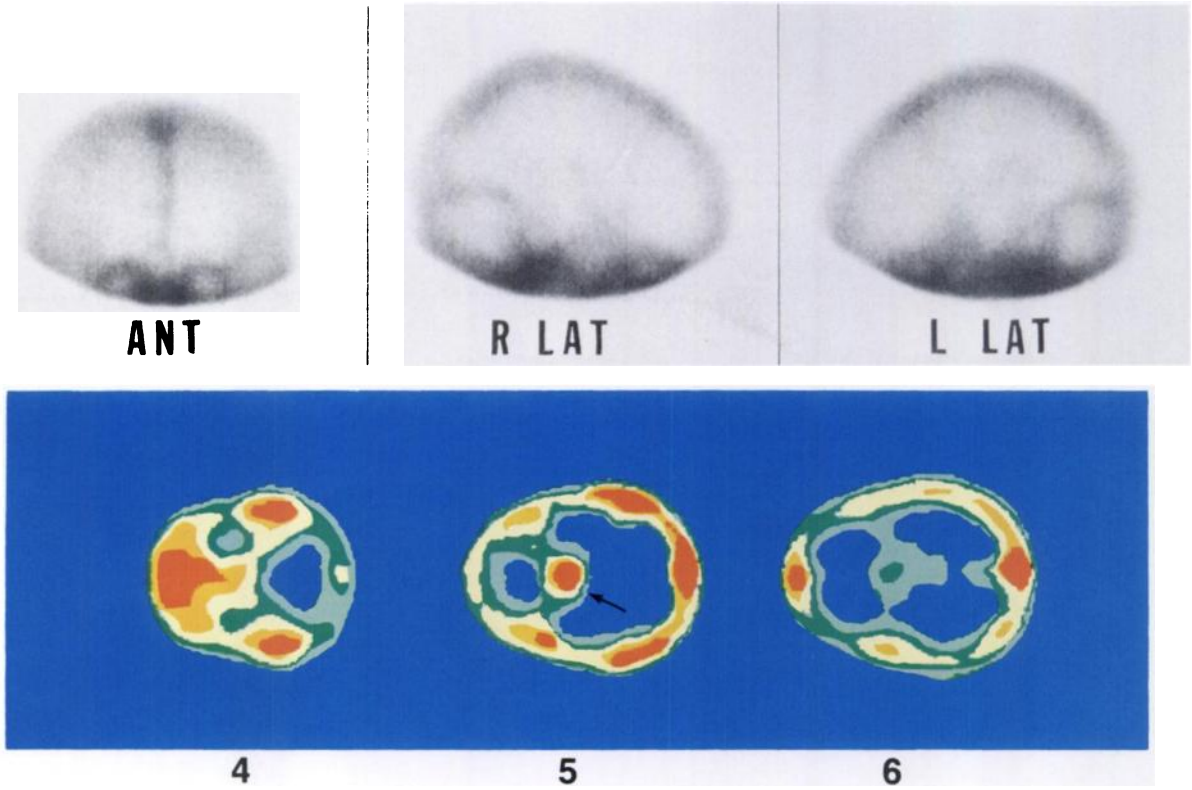

FIG. 9. Twelve-year-old girl. Craniopharyngioma (arrow).

sions contain increased radioactivity. Neither lesion is visualized in the standard scintigrams, but both are obvious in the RCT section. When the phantom was imaged with spheres containing no activity (Fig. 5B), neither lesion was visible in the standard view, and the smaller "cold" lesion was difficult to see in the RCT section. Standard analog scintigrams of the phantom did not improve the lesion detectability over the digital presentations shown here.

For an initial clinical evaluation, 65 patients with a high suspicion of brain lesions had routine brain scanning and RCT imaging. In 40 of these patients the radionuclide scan and RCT images were normal. The results in patients with metastatic carcinoma of the lung, penetrating orbital knife injury, cerebrovascular accident, and craniopharyngioma are shown in Figs. 6–9. Lesion-to-background ratios were used to compare standard scintigraphy to RCT in the 25 patients who had positive brain scans. The results are listed in Table 1 along with the final clinical diagnosis. On the average, the RCT lesion contrast was superior by a factor of more than 2 compared to the best view of the standard scintigrams.

To investigate the potential application of RCT to such other areas as the heart, an experimentally infarcted dog's heart was imaged following injection of ^{99m}Tc-MAA into the left atrium (Fig. 10). The heart was then removed and placed in a water-filled 9-in.-diam cylindrical container for the RCT data collection. The heart was then sectioned to correspond with the tomographic levels, and each of the gross sections was also imaged on the face of the collimator of the RCT camera in the nontomographic mode. Note the similarity between the tomographic and conventional images, with the infarct involving most of the posterior wall of the heart. Such information in patients could be of significant value in more precisely localizing myocardial abnormalities and in quantitating infarct size.

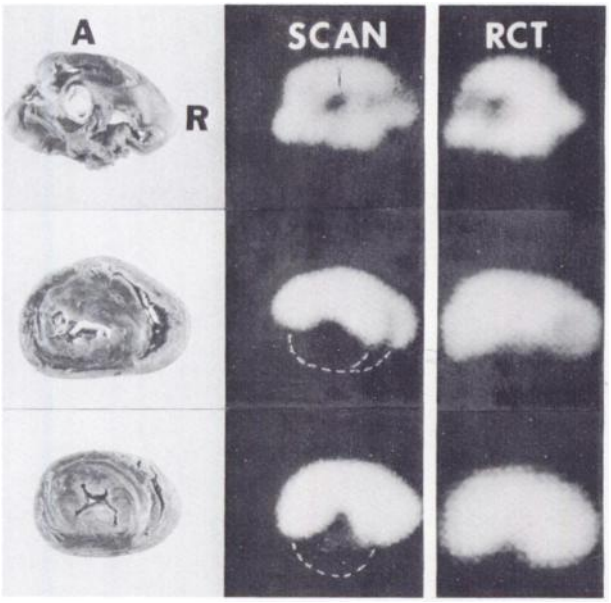

FIG. 10. Images of infarcted dog's heart following injection of ^{99m}Tc-MAA into left atrium. Infarct involves entire posterior wall of both ventricles (dotted line). Gross sections (left) correspond approximately to RCT levels (right). Scintillation-camera image of gross sections (center) is provided for comparison. For RCT data collection, heart was excised and imaged in 9-in.-diam water phantom.

CONCLUSIONS

In this feasibility study of RCT imaging in patients with brain lesions, we regularly obtained better image

TABLE 1. RCT LESION CONTRAST

Patient	Lesion-to-background ratios* RCT	Standard scintigram	Relative contrast (RCT/scintiphoto)	Diagnosis
1	1.52	0.52	3.0	Leukemic infiltration
2	0.63	0.37	1.7	Knife wound, right orbit
3	1.97	0.51	3.9	Arteriovenous malformation
4	0.92	0.60	1.5	Cerebral embolism
5	0.66	0.21	3.1	Subdural hematoma
6	1.10	0.60	1.8	Astrocytoma
7	1.73	1.47	1.2	Intracerebral hemorrhage (aneurysm)
8	0.92	0.50	1.8	Cerebral embolism
9	0.73	0.47	1.6	Intracerebral hematoma
10	1.08	0.56	1.9	Metastatic carcinoma (lung)
11	2.10	0.95	2.2	Metastatic carcinoma (breast)
12	1.43	0.58	2.5	Astrocytoma
13	2.26	0.38	5.9	Glioblastoma multiforme
14	2.08	0.74	2.8	Metastatic carcinoma
15	2.89	0.95	3.0	Metastatic carcinoma
16	4.83	2.65	1.8	Subdural hematoma
17	0.64	0.22	2.9	Cerebral infarction
18	1.64	0.37	4.4	Metastatic carcinoma (lung)
19	1.5	0.51	2.9	Metastatic carcinoma
20	1.21	0.40	3.0	Subdural hematoma
21	1.81	0.52	3.5	Metastatic carcinoma
22	1.47	0.97	1.5	Glioblastoma multiforme
23	2.01	0.39	5.1	Astrocytoma
24	2.84	1.87	1.5	Chronic subdural hematoma
25	0.49	0.11	4.4	Intracerebral hemorrhage
		Average	2.8	

* Lesion-to-background ratio (lesion counts — background counts)/background counts.

contrast than with standard scintigrams. In addition, the presentation of images in cross section permits a more precise determination of the location and extent of an abnormality. The encouraging results in this study have led us to begin the construction of a total-body system for imaging larger body areas such as heart, lung, liver, spleen, pancreas, and kidney.

ACKNOWLEDGMENTS

We would like to acknowledge the valuable contributions to this study by the following individuals: W. White, R. Sonnemaker, F. Whitehead, G. Engelmohr, A. Smudde, and V. Alagarsamy.

Portions of this material were presented at the 23rd Annual Meeting of the Society of Nuclear Medicine, held in Dallas, Texas, June, 1976.

REFERENCES

1. HOUNSFIELD GN: Computerized transverse axial scanning (tomography): Part 1. Description of system. *Br J Radiol* 46: 1016–1022, 1973

2. AMBROSE J: Computerized transverse axial scanning (tomography): Part 2. Clinical application. *Br J Radiol* 46: 1023–1047, 1973

3. KUHL DE, EDWARDS RQ: Image separation radioisotope scanning. *Radiology* 80: 653–661, 1963

4. BUDINGER TF, GULLBERG GT: Three-dimensional reconstruction in nuclear medicine emission imaging. *IEEE Trans Nucl Sci* 21: 2–20, 1974

5. BROOKS RA, DICHIRO G: Theory of image reconstruction in computed tomography. *Radiology* 117: 561–572, 1975

6. KUHL DE, EDWARDS RQ, RICCI AR, et al.: The Mark IV system for radionuclide computed tomography of the brain. *Radiology* 121: 405–413, 1976

7. MUEHLLEHNER G, BUCHIN MP, DUDEK JH: Performance parameters of a positron imaging camera. *IEEE Trans Nucl Sci* 23: 528–537, 1976

8. HOFFMAN EJ, PHELPS ME, MULLANI NA, et al.: Design and performance characteristics of a whole-body positron transaxial tomograph. *J Nucl Med* 14: 493–502, 1976

9. KEYES JW, ORLANDEA N, HEETDERKS WJ: Emission CAT scanning—Progress on a system based on the gamma camera. *Proceedings of the Sixth Symposium on Sharing of Computer Programs and Technology in Nuclear Medicine, Atlanta, Georgia, January 25–26, 1976*, Howard BY, ed. New York, Society of Nuclear Medicine, 1976, pp 314–320

10. MUEHLLEHNER G, WETZEL RA: Section imaging by computer calculation. *J Nucl Med* 12: 76–84, 1971

11. KAY DB, KEYES JW, SIMON W: Radionuclide tomographic image reconstruction using Fourier transform techniques. *J Nucl Med* 15: 981–986, 1974

12. OPPENHEIM BE, HOFFER PB, GOTTSCHALK A: Nuclear imaging: A new dimension. *Radiology* 118: 491–494, 1976

13. OPPENHEIM BE: More accurate algorithms for iterative three-dimensional reconstruction. *IEEE Trans Nucl Sci* 21: 72–77, 1974

14. DE ROSIER DJ, KLUG A: Reconstruction of three-dimensional structures from electron micrographs. *Nature* 217: 130–134, 1968

15. PETERS TM, SMITH PR, GIBSON RD: Computer aided transverse body-section radiography. *Br J Radiol* 46: 314–317, 1973

16. MERSEREAU RM, OPPENHEIM AV: Digital reconstruction of multidimensional signals from their projections. *Proc. IEEE* 62: 1319–1337, 1974

17. BRACEWELL RN, RIDDLE AC: Inversion of fan-beam scans in radio astronomy. *Astrophys J* 150: 427–434, 1967

18. KLUG A, CROWTHER RA: Three-dimensional image reconstruction from the viewpoint of information theory. *Nature* 238: 435–440, 1972